Role of oxygen partial pressure and seed layer chemistry in flux mediated epitaxy of single phase multiferroic $BiFeO_3$ thin films

Varatharajan Anbusathaiah,[1,a)] Ching Jung Cheng,[1] Sung Hwan Lim,[2] Makoto Murakami,[2] Lourdes G. Salamanca-Riba,[2] Ichiro Takeuchi,[2] and Valanoor Nagarajan[1,b)]
[1]*School of Materials Science and Engineering, University of New South Wales, Sydney, New South Wales 2052, Australia*
[2]*Department of Materials Science and Engineering, University of Maryland, College Park, Maryland 20742, USA*

(Received 10 September 2008; accepted 18 October 2008; published online 11 November 2008)

Multiferroic $BiFeO_3$ (BFO) thin films have been fabricated via flux mediated epitaxy with varying oxygen partial pressure and flux composition (Bi_2O_3:CuO) conditions. Transmission electron microscopy coupled with energy dispersive x-ray spectroscopy as well as piezoresponse force microscopy confirm, that with the correct flux and seed layer conditions, even at very low partial pressures (3 mTorr) no secondary phases are formed. The study reveals the crucial role of the bottom seed layer and flux chemistry in epitaxy of BFO thin films and provides alternate routes to BFO epitaxy in oxygen-deficient environments. © *2008 American Institute of Physics*.
[DOI: 10.1063/1.3021021]

Bismuth ferrite ($BiFeO_3$ or BFO)-based thin films have recently generated great attention due to promising multiferroic properties.[1,2] As bismuth (Bi) is a highly volatile element, BFO thin film deposition requires the use of Bi-excess targets or precursors to compensate for the Bi loss at the nominally employed high growth temperatures (>550 °C). As such the optimized growth window for BFO and especially in thin-film form is extremely stringent.[3] Even slightly excess Bi potentially leads to Bi_2O_3 pockets[4] and since Bi_2O_3 is a good ionic conductor (δ-$Bi_2O_3 \sim 1\ \Omega$ cm at 800 °C), it can result in high leakage-current density. On the other hand, Bi-deficient films tend to easily form two-phase mixtures comprising of BFO and secondary Fe_2O_3.[4,5] It has been argued that such secondary phases question the use of BFO thin films as a model material to investigate multiferroicity.[4,6]

Recently, we demonstrated that BFO thin films deposited via pulsed laser flux mediated epitaxy (FME) (Ref. 7) show enhanced ferroelectric and dielectric properties without any secondary or parasitic phases thus presenting FME as a solution to the phase-purity challenge. In FME,[8–10] a flux compound (in this case Bi_2O_3–CuO) is used to reduce the melting point at the surface and forms a reservoir of Bi required to maintain the film stoichiometry. The vapor ablated from the target material meets the flux on the surface of the substrate, diffuses into the liquid intermediate phase, and finally nucleates on a predeposited seed layer. Since the flux serves as to replenish volatile Bi, low oxygen pressures (and hence cleaner environments) are possible, thereby making this approach tenable for even processes such as molecular beam epitaxy. Of significance is that the liquid phase yields a very large grain size,[10] which can drastically improve dielectric response. Indeed, in our previous work,[7] phase-pure films with much enhanced dielectric properties and superior leakage-current resistance were deposited at oxygen partial pressures as low as 5 mTorr with grain sizes of the order of 1–2 μm. Here we delineate the crucial role of flux and seed layer chemistry during the FME process in obtaining phase-pure BFO thin films by systematically varying oxygen partial pressure and flux composition.

The BFO thin films used in this study were deposited on $SrRuO_3$ (SRO) buffered (001) oriented $SrTiO_3$ (STO) substrates using 10% Bi-excess $Bi_{1.1}FeO_3$ targets via pulsed laser (KrF excimer laser $\lambda = 248$ nm) ablation. The thicknesses, the growth temperature, and the composition of the flux were kept identical to the previous work;[7] the thicknesses of the BFO thin film (200 nm), flux (40 nm), and seed bottom BFO layer (10 nm) were kept constant in all the samples. Growth temperatures were maintained at 650 °C for the seed layer and flux deposition and 730 °C for the BFO layer. Two different flux compositions (11.7 and 17 vol % of CuO) were used, and the oxygen partial pressure during deposition was 3–30 mTorr. Ferroelectric domain structure was investigated using piezoresponse force microscopy (PFM). Details of the tip and imaging conditions are given elsewhere.[11] Cross sectional transmission electron microscopy (TEM) (XTEM) and energy dispersive x-ray spectroscopy (EDS) analysis were obtained using the Philips CM200 TEM operated at an accelerating voltage of 200 kV. For the EDS scans, images were captured before and after each scan and only those scans that did not show drift were considered for further analysis.

Figure 1 shows a series of the topographic and PFM images obtained on the FME grown BFO thin films. Figure 1(a) shows the topography of the BFO thin films whose oxygen partial pressure for the entire layers of film (bottom seed layer, flux, and BFO film) has been maintained at 30 mTorr and the CuO content in the flux was at 11.7% (sample 1). Compared to the BFO thin film grown with a conventional pulsed laser deposition on the same SRO/STO system, the sizes of the grains are relatively very large varying from 1 to 5 μm. The simultaneously captured out-of-plane PFM (OP-PFM) image of this as-grown state is shown in Fig. 1(b). Writing experiment, where a dc bias of −10 V was applied to its central $3 \times 3\ \mu m^2$ region, followed by reverse

a)Electronic mail: anbu@materials.unsw.edu.au.
b)Electronic mail: nagarajan@unsw.edu.au.

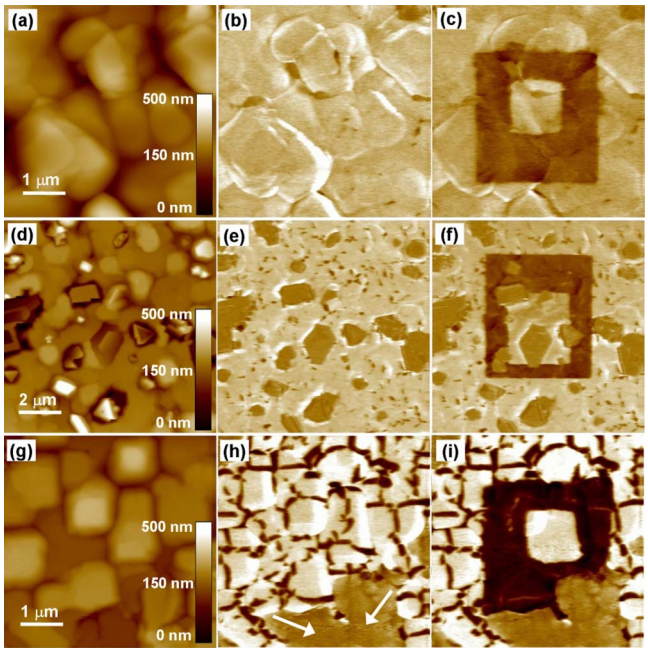

FIG. 1. (Color online) PFM analysis of the BFO thin films. (a), (d), and (g) are topography images of samples 1, 2, and 3, respectively. (b), (e), and (h) are the simultaneously captured out-of-plane PFM (OP) image at its as-grown state, respectively for each sample. [(c), (f), and (i)] The OP PFM image of the same region after applying −5 V (outer square) and +5 V (inner square) dc biases at the center of the region.

bias (+10 V) in a 1×1 μm^2 area, was used to probe the domain switching behavior. The OP-PFM image after applying the dc biases shows distinct domain contrasts [Fig. 1(c)] and hence clearly shows ferroelectric domain switching. For the second BFO thin films, the growth pressure was 30 mTorr and the CuO content in the flux was increased to 17 vol % (sample 2). The surface topography [Fig. 1(d)] of the surface shows a large amount of flux that remains over the film surface. XTEM analysis (will be discussed later) revealed that these deposits grow from within the film and hence can be linked to the initial seed layer. For this film, the OP-PFM before [Fig. 1(e)] and after positive and negative writings [Fig. 1(f)] shows that regions between the flux deposits again have good ferroelectric domain switching. Most importantly, we note that the flux regions remain unaltered to the external electrical perturbation. In the case of third BFO thin films, with lower oxygen partial pressure (3 mTorr) and low CuO (11.7%) in the flux composition (sample 3), the topography is shown in Fig. 1(g). Contrary to the first case and despite using low CuO content, this film also shows a flux region on the surface. The OP-PFM image [Fig. 1(h)] captured simultaneously confirms that these regions constitute the nonferroelectric flux particles which are indicated out by arrows, and similar to Fig. 1(f) the flux region remains inert to the applied electric field [Fig. 1(i)]. Thus the strong role of both oxygen partial pressure as well as flux chemistry is evident in determining the ultimate phase as well as surface properties of the BFO thin film.

Systematic XTEM analyses were carried out on all the three samples to understand interfacial chemistry and its resultant effects on microstructure as well as phase behavior. Figure 2(a) shows the XTEM bright field image of BFO sample 1, with the selected area diffraction pattern (SADP) shown in the inset. This image, along with the SADP, reveals

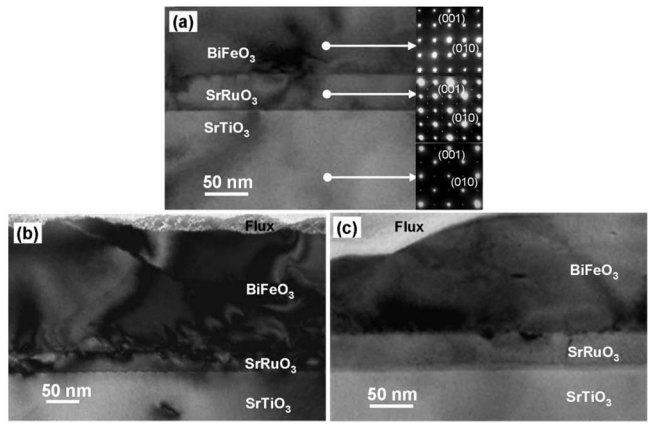

FIG. 2. (a) XTEM image of sample 1. The inset shows the SADP of the each layer. (b) The XTEM image of sample 2 and (c) sample 3 of the FME-BFO thin films.

that the BFO thin film is epitaxial with sharp interfaces, and no evidence of an interfacial layer between the seed BFO and the top BFO layer was observed. The SADP confirms the presence of single phase BFO thin films without any secondary phases previously observed for such partial pressures.[3,4] This is the ideal case of FME and complete structural details can be found in Ref. 7. Figure 2(b) (BFO sample 2 with excess CuO in the flux) shows a highly strained interface between the BFO and the SRO with secondary phase inside the BFO matrix. In agreement with the atomic force microscopy/PFM observation, the surface of this BFO thin film is relatively rough and it shows a significant amount of residual flux. There are distinct threading dislocations across the entire interface (from the strain contrast), and they may be the consequence of the breakdown of the delicate flux-BFO equilibria at the growing surface.[3]

Figure 3(a) represents the bright field elastic TEM image and corresponding EDS maps (Cu *K* [Fig. 3(b)], Bi *L* [Fig.

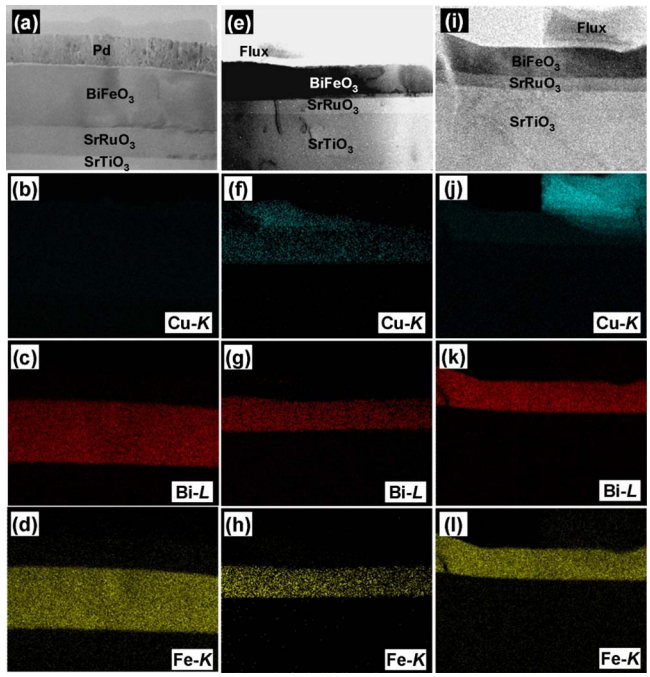

FIG. 3. (Color online) Bright-field elastic TEM image with EDS maps for the Cu *K*, Bi *L*, and Fe *K*. (a)–(d) for sample 1; (e)–(h) for sample 2; and (i)–(l) for sample 3.

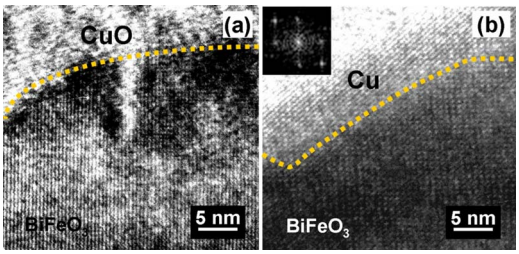

FIG. 4. (Color online) High resolution TEM (HRTEM) image of the flux-film interface layer (a) for sample 2 and (b) for sample 3. The inset to (b) is the optical-diffraction pattern confirming the fcc structure for the Cu flux.

3(c)], and Fe *K* [Fig. 3(d)] for sample 1. It shows phase-pure BFO without any traces of flux material (mainly Cu) observed inside the BFO matrix. Figures 3(e)–3(h) are the similar series of images which belongs to the flux-BFO sample 2. From these images, it is seen that the Cu is dispersed into the BFO film and is also present as a flux residue on the top surface, while EDS maps for the Bi and Fe show their presence only in the film. The inhomogeniety in composition and poor sample interface is attributed to the failure of quasi-equilibrium state between the growing film and the liquid flux, which in turn results in a variation in the flux composition. The binary solid-solubility phase diagram[12] for Bi_2O_3–CuO shows a relatively deep eutectic point at 90% Bi_2O_3 and a melting point of ~600 °C. For CuO volume fractions outside this eutectic point, the flux surface has a much higher melting point, and the growing interface is comprised of liquid with solid solution precipitates of Bi_2O_3–CuO. The growth problem is further compounded as the seed BFO thin film is grown at conditions of O_2 partial pressure and temperature (650 °C) that stabilize Bi_2O_3.[3,4] At equilibrium, when the flux layer is deposited on this seed BFO layer, the seed layer acts as a reservoir for Bi_2O_3 and hence changes the fraction of Bi_2O_3 in the liquid flux. This process effectively changes the effective vol % of the CuO and hence raises the melting point; thus there is no driving force for the phase separation of Bi_2O_3 from the flux. Thus, when a BFO thin film is deposited via this Bi_2O_3 rich flux mediator, the CuO remains at the matrix without any phase separation (due to the higher melting point and excess Bi_2O_3) to form a CuO capping layer. High-resolution TEM (Fig. 4) and local EDS analysis confirms this hypothesis, with both Cu and O counts being recorded. This explains why the film with 17% CuO displays such poor interfaces contrary to those grown with 11% CuO flux; as both samples 1 and 2 have identical seed layer oxygen partial pressure conditions, it underlines the crucial role of the flux chemistry.

For sample 3 BFO thin film, although the XTEM image [Fig. 2(c)] shows sharp interfaces without any strained region, it also shows flux on the top of the film surface. The flux distribution is low compared to sample 2 of FME-BFO thin films. From the phase diagram proposed for BFO deposition,[3,4] one could expect that the 10 nm thick seed BFO layer at 3 mTorr and 650 °C be Bi and O deficients. Hence the flux now acts like a reservoir for both Bi and O, and efficient separation of Bi_2O_3 takes place. This would result in Cu and not CuO being left as a residue. Indeed the EDS map [Fig. 3(j)] for Cu reveals that it is present only in the top flux layer and not in the BFO film and simultaneously obtained EDS spectra of Bi *L* [Fig. 3(k)] and Fe *K* ions [Fig. 3(l)] for this sample show sharp interfaces with their presence only in the BFO layer. Furthermore, point EDS on the BFO layer indeed confirmed that the atomic percentage of the Bi to Fe ratio in BFO layer is 1:1. Thus, the thin film deposited at low O_2 partial pressure and low CuO percent maintains the stoichiometric ratio of the BFO.

The distinct difference in the chemical as well as the structural nature of the residual flux on the surface of these thin films is further corroborated by high resolution TEM (HRTEM) analyses focused on the flux (Fig. 4). The HRTEM image for sample 2 [Fig. 4(a)] of the flux-film interface that reveals the flux remaining on the surface is amorphous; on the other hand the HRTEM image [Fig. 4(b)] for sample 3 thin film shows well-defined lattice fringes, and the selective area optical-diffraction pattern of the flux region (inset) shows a pattern characteristic of a fcc structure. Using commercial software such as CARINE as well as web-based diffraction analysis[13] we confirmed that none of the possible oxides of Cu have a cubic structure. On the other hand the pattern matches very well with that expected for metallic Cu. Point EDS also confirmed that the flux layer in sample 3 is devoid of any oxygen. Conversely for sample 2, combining the above finding [Fig. 4(a)] with the fact that point EDS found residual oxygen in the flux, we conclude that CuO has remained as is without any separation, thereby causing a failure of the delicate vapor-liquid equilibrium and thus revealing the practical limits of the FME technique.

Research at UNSW was supported by an ARC-DP0666231 and a DEST ISL grant. Work at UMD was supported by access to the Shared Experimental Facilities of the UMD-NSF-MRSEC (DMR 0520471), NSF (DMR 0603644), and ARO (W911NF-07-1-0410). The work was also supported by the W. M. Keck Foundation, NEDO, and the Maryland Nanocenter.

[1] W. Eerenstein, N. D. Mathur, and J. F. Scott, Nature (London) **442**, 759 (2006).
[2] R. Ramesh and N. A. Spaldin, Nature Mater. **6**, 21 (2007).
[3] H. Bea, M. Bibes, S. Fusil, K. Bouzehouane, E. Jacquet, K. Rode, P. Bencok, and A. Barthelemy, Phys. Rev. B **74**, 020101 (2006).
[4] H. Bea, M. Bibes, A. Barthelemy, K. Bouzehouane, E. Jacquet, A. Khodan, J. P. Contour, S. Fusil, F. Wyczisk, A. Forget, D. Lebeugle, D. Colson, and M. Viret, Appl. Phys. Lett. **87**, 072508 (2005).
[5] M. Murakami, S. Fujino, S. H. Lim, L. G. Salamanca-Riba, M. Wuttig, I. Takeuchi, B. Varughese, H. Sugaya, T. Hasegawa, and S. E. Lofland, Appl. Phys. Lett. **88**, 112505 (2006).
[6] W. Eerenstein, F. D. Morrison, J. Dho, M. G. Blamire, J. F. Scott, and N. D. Mathur, Science **307**, 1203 (2005).
[7] S. H. Lim, M. Murakami, J. H. Yang, S. Y. Young, J. Hattrick-Simpers, M. Wuttig, L. G. Salamanca-Riba, and I. Takeuchi, Appl. Phys. Lett. **92**, 012918 (2008).
[8] R. Takahashi, Y. Tsuruta, Y. Yonezawa, T. Ohsawa, H. Koinuma, and Y. Matsumoto, J. Appl. Phys. **101**, 033511 (2007).
[9] R. Takahashi, Y. Yonezawa, M. Ohtani, M. Kawasaki, K. Nakajima, T. Chikyow, H. Koinuma, and Y. Matsumoto, Adv. Funct. Mater. **16**, 485 (2006).
[10] J. F. Ihlefeld, W. J. Borland, and J. P. Maria, Adv. Funct. Mater. **17**, 1199 (2007).
[11] V. Anbusathaiah, V. Nagarajan, and S. Aggarwal, Appl. Phys. Lett. **89**, 132912 (2006).
[12] *Phase Diagrams for Ceramists*, edited by E. M. Levin and H. F. McMurdie (American Ceramic Society, Columbus, Ohio, 1964), Vol. 3, p. 20 (1964).
[13] Web Electron Microscopy Applications Software (WEBEMAPS).